

# Laminar mixing, heat transfer and pressure drop in tree-like microchannel nets and their application for thermal management in polymer electrolyte fuel cells

S.M. Senn, D. Poulikakos\*

*Laboratory of Thermodynamics in Emerging Technologies, Department of Mechanical and Process Engineering,  
ETH Swiss Federal Institute of Technology Zurich, ETH Zentrum, CH-8092 Zurich, Switzerland*

Received 14 June 2003; received in revised form 1 December 2003; accepted 8 December 2003

## Abstract

The laminar convective heat transfer and pressure drop characteristics in tree-like microchannel nets are numerically investigated and compared to the corresponding characteristics in traditional serpentine flow patterns, by solving the Navier–Stokes and energy equation for an incompressible fluid with constant properties in three dimensions. A constant heat flux is applied to the walls of the square cross-sectional channels. The intrinsic advantage of tree-like nets with respect to both heat transfer and pressure drop is demonstrated. In addition, secondary flow motions initiated at bifurcations and their important role on thermal mixing are identified and discussed. Thermal management issues in polymer electrolyte fuel cells are addressed and in this context, the future employment of tree nets is recommended.

© 2004 Elsevier B.V. All rights reserved.

*Keywords:* Deterministic tree networks; Microchannels; Secondary flows; Laminar mixing; Thermal management; PEM fuel cells

## 1. Introduction

Effective thermal and water management in polymer electrolyte fuel cells is key to ensure high cell performance and efficiency. The irreversibility of electrochemical reactions and joule heating are the most important factors causing heat generation inside PEM fuel cells. The temperature distribution in the cell has a strong impact on the cell performance since it influences the water distribution by means of condensation and affects the multicomponent gas diffusion transport characteristics through thermocapillary forces and thermal buoyancy. Also, the kinetics of electrochemical reactions directly depends on temperature. Excessive global or local cell temperature due to insufficient or non-effective cell cooling may cause membrane dehydration, shrinking or even rupture. Membrane hydration is important to ensure high proton conductivity and thus cell performance. Hence, thermal and water management issues are strongly coupled and they have a direct impact on cell performance. Thermal management includes the removal of the generated heat from inside the cell to the outside. Further, a temporally and spatially uniform temperature distribution must be provided, hot spots need to be avoided, and pumping power required

for the coolant circulation has to be minimized in order to ensure high overall cell efficiency. Therefore, pressure drop must be minimized while maximizing the heat transfer capability at the same time.

For thermal management in PEM fuel cell stacks, usually serpentine or meander cooling patterns are used, having only one or a few inlets and outlets, for liquid or gas coolant, depending on the system design and the cell size. For overall stack functionality reasons, the number of fluid inlets and outlets must be small, making parallel cooling patterns usually inappropriate. These circumstances call for a flow geometry with minimum flow resistance between a volume and one point, i.e. between the inside of the cell and the inlet or outlet. In this paper, the use of deterministic tree networks of Bejan [1,2], also termed as fractal networks of branching tubes [3], is suggested for this purpose. Bejan and Errera [4] discussed a deterministic tree network for fluid flow with minimum flow resistance between a volume and a point, subjected to two constraints: fixed total volume and fixed channel volume. Bejan [5] showed that the total heat current convected by a double tree is proportional to the total volume raised to power 3/4. Chen and Cheng [6], following the principles put forth by Bejan [1,2,5], presented an analytical study on the heat transfer and pressure drop characteristics in fractal tree-like microchannel nets in which a comparison is made between fractal nets and traditional

\* Corresponding author. Tel.: +41-1-632-2738; fax: +41-1-632-1176.  
E-mail address: [dimos.poulikakos@ethz.ch](mailto:dimos.poulikakos@ethz.ch) (D. Poulikakos).

**Nomenclature**

$a$	distance (m)
$Br$	Brinkman number (–)
$c_p$	specific heat capacity ( $\text{J kg}^{-1} \text{K}^{-1}$ )
$d$	channel diameter (m)
$Ec$	Eckert number (–)
$f$	Moody (or Darcy) friction factor (–)
$h$	heat transfer coefficient ( $\text{W m}^{-2} \text{K}^{-1}$ )
$k$	branching level (–)
$L$	channel length (m)
$m$	total number of branching levels (–)
$\dot{m}$	mass flow rate ( $\text{kg s}^{-1}$ )
$n$	parameter (–)
$Nu$	Nusslet number (–)
$p$	pressure (Pa)
$Pr$	Prandtl number (–)
$q''$	wall heat flux ( $\text{W m}^{-2}$ )
$r$	length ratio (–)
$Re$	Reynolds number (–)
$S$	surface area ( $\text{m}^2$ )
$t$	time (s)
$T$	temperature (K)
$v$	velocity ( $\text{m s}^{-1}$ )
$x, y, z$	coordinates (m)

**Greek letters**

$\beta$	channel diameter ratio (–)
$\gamma$	channel length ratio (–)
$\lambda$	thermal conductivity ( $\text{W m}^{-1} \text{K}^{-1}$ )
$\mu$	dynamic viscosity (Pa s)
$\xi, \eta, \zeta$	coordinates (m)
$\rho$	density ( $\text{kg m}^{-3}$ )

**Subscripts**

$i, j$	indices (Einstein summation convention)
in	inlet
$k$	branching level
m	mean
max	maximum
min	minimum
ref	reference
w	wall
$\xi_k$	in $\xi_k$ direction where $k$ indicates the branching level
0	zeroth branching level

**Superscript**

$\sim$	dimensionless
--------	---------------

In the course of electronics miniaturization during the last decade, denser component packing led to higher energy dissipation rates and necessitated the demand for high-performance micro heat exchangers consisting of microchannel systems being based on gas or liquid convective heat transfer in single or two-phase flow regimes [7–9]. Compared to large diameter channels, the large surface to volume ratio of small diameter channels provides a better heat transfer capability and therefore makes microchannel systems attractive for dealing with high heat fluxes. However, a penalty is paid due to the higher pressure drop, caused again by the increased surface to volume ratio. In the literature, microchannels are generally defined as channels having a hydraulic diameter smaller than 1 mm and larger than  $1 \mu\text{m}$  [7].

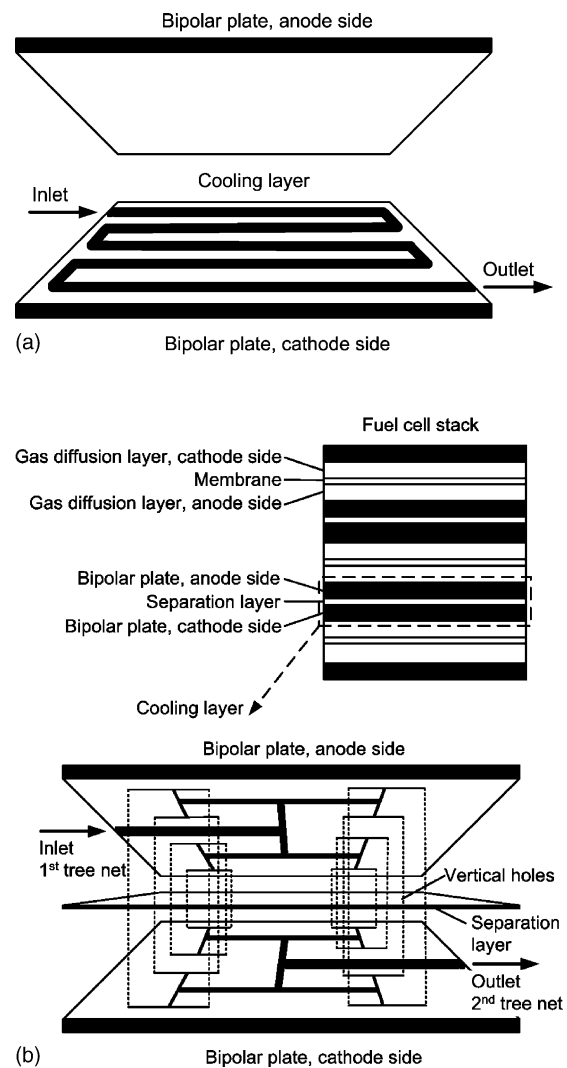


Fig. 1. Thermal management in polymer electrolyte fuel cell stacks. (a) Traditional serpentine or meander cooling patterns without a separation layer between the bipolar plates. (b) Superimposed tree nets. One net is imposed on the backside of the anode bipolar plate and another net is imposed on the backside of the cathode bipolar plate. The two nets are separated by a separation layer. Vertical holes in this layer connect the ends of the highest branching levels to each other.

parallel channels. After simplifying assumptions including neglecting the effect of bifurcation on pressure drop and heat transfer they found that the considered fractal nets provide higher heat transfer capability and cause less pressure drop.

A substantial research effort has been focused on the experimental [10–17,19,21] and numerical [18–24] investigation of single phase flow in such microchannels. Most of this work described in literature is concerned with two parameters, the friction factor and the heat transfer coefficient, regarding channels with diameters between  $1\ \mu\text{m}$  and  $1\ \text{mm}$ . Experimental results show agreement but also substantial deviation from classical theory developed for larger channels. Possible reasons for the measured deviations are discussed and investigated in the literature [25–33]: measurement inaccuracy at the micro-scales, high relative surface roughness at the channel walls, the electric double-layer (EDL) effect, viscous heating, and slip-flow for gases at high Knudsen numbers. Due to the large surface to volume ratio, surface related phenomena become important or rather dominant at the micro-scales and they might not be neglected, as at the larger scales. However, the literature is not conclusive with respect to the dependence of the above mentioned two parameters on the hydraulic diameter in the submicron-scales. A key property of a tree net is that there is not an intrinsic length-scale, defined in an ad hoc manner. Such scales are reduced from one branching level to the next higher one, such that the relative importance of different phenomena depends on the branching level.

In this paper, a numerical analysis of the fundamental heat transfer and pressure drop characteristics in tree-like microchannel nets as shown in Figs. 1 and 2 is presented.

The future application of tree nets for thermal management in PEM fuel cells is suggested and discussed, among other application areas. In the analytical work by Chen and Cheng [6], the effect of bifurcation on heat transfer and pressure drop is neglected and it is assumed for simplicity, that the laminar flow is fully developed both thermally and hydrodynamically. Such assumptions are appropriate if for the flow channels, the length to diameter ratio is very high and the Reynolds number is rather small, such that the hydrodynamic and thermal development lengths can be neglected compared to the channel lengths. The present computational study is not based on such assumptions and it takes into account important hydrodynamic and thermal effects from bifurcations, such as secondary flow motions and convective thermal mixing. The Navier–Stokes equations and the energy equation are numerically solved in three dimensions in conjunction with a constant heat flux boundary condition at the channel walls. The characteristic variations of the Nusslet number and the friction factor along the tree net are discussed and compared to the ones of a serpentine flow pattern having the same heat transfer surface area.

## 2. Mathematical model

In the following mathematical model, an incompressible fluid is assumed with constant viscosity  $\mu$ , constant heat

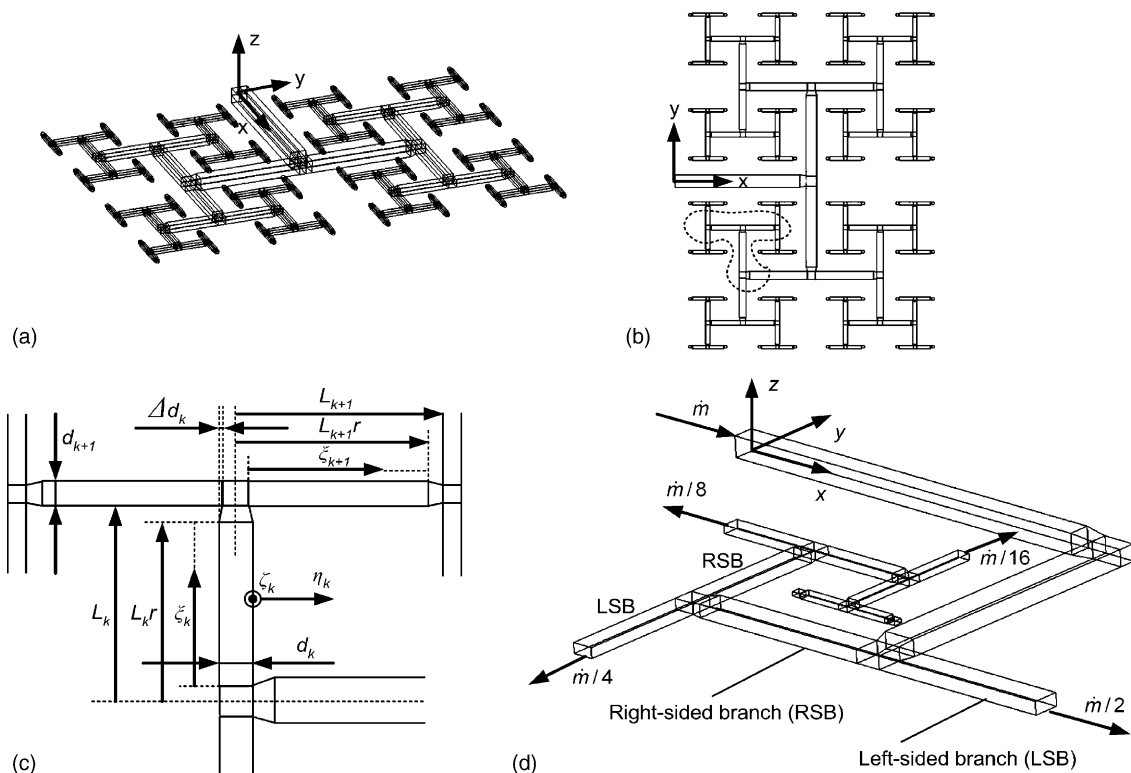


Fig. 2. Tree net with six branching levels  $m = 6$ ,  $\beta = d_{k+1}/d_k = 2^{-1/3}$ ,  $\gamma = L_{k+1}/L_k = 2^{-1/2}$ ,  $L_0/d_0 = 10$ ,  $r = 0.95$ , and  $\Delta d_k = a_k$ . (a) Three-dimensional view. (b) Top view. (c) Schematic of the geometric structure of the tree net. (d) Computational domain with inlet and outlet mass flow rates.

capacity  $c_p$ , and constant thermal conductivity  $\lambda$ . Using the Einstein summation convention, continuity reads

$$\frac{\partial v_j}{\partial x_j} = 0, \quad (1)$$

momentum conservation is written as

$$\begin{aligned} \frac{\partial}{\partial t}(\rho v_i) + \frac{\partial}{\partial x_j}(\rho v_j v_i) \\ = -\frac{\partial p}{\partial x_i} + \frac{\partial}{\partial x_j} \left( \mu \frac{\partial v_i}{\partial x_j} \right), \quad i = 1, 2, 3, \end{aligned} \quad (2)$$

and the energy equation including the viscous dissipation term is given by

$$\begin{aligned} \frac{\partial}{\partial t}(\rho T) + \frac{\partial}{\partial x_j}(\rho v_j T) \\ = \frac{\partial}{\partial x_j} \left( \frac{\lambda}{c_p} \frac{\partial T}{\partial x_j} \right) + \frac{\mu}{c_p} \left( \frac{\partial v_i}{\partial x_j} + \frac{\partial v_j}{\partial x_i} \right) \frac{\partial v_i}{\partial x_j}. \end{aligned} \quad (3)$$

For a non-dimensional representation of the problem, the hydraulic channel diameter  $d_0$  of the zeroth branching level is used as a length-scale, the inlet velocity  $v_{in}$  is used as a velocity scale, the inlet temperature  $T_{in}$  and a maximum temperature  $T_{max}$  are used for temperature scaling, and pressure is scaled through a reference pressure  $p_{ref}$ :

$$\begin{aligned} \tilde{x}_i \equiv \frac{x_i}{d_0}, \quad \tilde{t} \equiv \frac{t v_{in}}{d_0}, \quad \tilde{v}_i \equiv \frac{v_i}{v_{in}}, \\ \tilde{T} \equiv \frac{T - T_{in}}{T_{max} - T_{in}}, \quad \tilde{p} \equiv \frac{p - p_{ref}}{\rho v_{in}^2}. \end{aligned} \quad (4)$$

The maximum temperature is defined as  $T_{max} = q'' S / (\dot{m}_{k=0} c_p) + T_{in}$ , where  $q''$  is the constant wall heat flux and  $S$  represents the corresponding heated surface area. Based on these scalings and the definition of non-dimensional numbers,

$$\begin{aligned} Re \equiv \frac{\rho v_{in} d_0}{\mu}, \quad Pr \equiv \frac{c_p \mu}{\lambda}, \\ Br \equiv \frac{\mu v_{in}^2}{\lambda (T_{max} - T_{in})}, \quad Ec \equiv \frac{Br}{Pr}, \end{aligned} \quad (5)$$

the conservation equations (1)–(3) can be written in non-dimensional form as

$$\frac{\partial \tilde{v}_j}{\partial \tilde{x}_j} = 0, \quad (6)$$

$$\frac{\partial}{\partial \tilde{t}} \tilde{v}_i + \frac{\partial}{\partial \tilde{x}_j} (\tilde{v}_j \tilde{v}_i) = -\frac{\partial \tilde{p}}{\partial \tilde{x}_i} + \frac{1}{Re} \frac{\partial^2 \tilde{v}_i}{\partial \tilde{x}_j \partial \tilde{x}_j}, \quad i = 1, 2, 3, \quad (7)$$

and

$$\begin{aligned} \frac{\partial}{\partial \tilde{t}} \tilde{T} + \frac{\partial}{\partial \tilde{x}_j} (\tilde{v}_j \tilde{T}) \\ = \frac{1}{Re Pr} \frac{\partial^2 \tilde{T}}{\partial \tilde{x}_j \partial \tilde{x}_j} + \frac{Br}{Re Pr} \left( \frac{\partial \tilde{v}_i}{\partial \tilde{x}_j} + \frac{\partial \tilde{v}_j}{\partial \tilde{x}_i} \right) \frac{\partial \tilde{v}_i}{\partial \tilde{x}_j}. \end{aligned} \quad (8)$$

### 3. Numerical solution

#### 3.1. Models and boundary conditions

Based on the above mathematical formulation, the fluid mechanics and heat transfer in a tree-like net consisting of channels with square cross-sections, as shown in Fig. 2, is computed. The fractal geometry considered here is fixed if the following independent parameters are given: the number of branching levels  $m$ , the ratio of the channel diameters  $\beta = d_{k+1}/d_k$  between two consecutive branching levels, the corresponding channel length ratio  $\gamma = L_{k+1}/L_k$ , the length to diameter ratio  $L_0/d_0$  at the zeroth branching level, the ratio  $r$  of the straight channel length and the entire channel length  $L_k$  including the length of the converging duct, and the length  $L_0$  or the diameter  $d_0$  at the zeroth branching level. In this study, a fractal geometry with  $m = 6$ ,  $\beta = 2^{-1/3}$ ,  $\gamma = 2^{-1/2}$ ,  $L_0/d_0 = 10$ ,  $r = 0.95$ , and  $d_0 = 1$  mm is investigated. Optimization of a single plane construct consisting of a T-shaped junction with respect to minimum flow resistance by fixing the total tube volume yields the optimal diameter ratio  $\beta = d_{k+1}/d_k = 2^{-1/3}$ , known as Murray's law [34,35], which is independent of the length ratio  $\gamma = L_{k+1}/L_k$  and geometry. If the space allocated to the construct is further fixed, i.e.  $2L_{k+1}L_k = \text{const.}$ , a second minimization of the flow resistance [5] yields the optimal length ratio  $\gamma = L_{k+1}/L_k = 2^{-1/3}$ . However, this length ratio creates the practical problem of channel overlapping for a right-angled plane construct with  $m > 4$ . To circumvent this,  $\gamma = 2^{-1/2}$  is chosen in this study. Such a tree net has one fluid inlet at the zeroth branching level and a number of  $2^m$  fluid outlets at the highest branching level, where  $m$  represents the total number of branching levels. A traditional heat removal concept for PEM fuel cells is shown in Fig. 1(a) in which a serpentine or meander flow pattern is manufactured into one of the bipolar plates.

An alternative concept utilizing the tree network of channels requires that on top of the first net, a second net of identical geometry is superimposed and the ends of the highest branching levels of each net are then vertically connected in order to build up a closed fractal tree, having one fluid inlet at the zeroth branching level of the first net and one fluid outlet at the zeroth branching level of the second net. A novel concept for thermal management in PEM fuel cell stacks which is based on this principle is presented in Fig. 1(b): A tree-like flow pattern (first tree net) is imposed on the backside of the anode bipolar plate and another net (second tree net) is imposed on the backside of the adjacent cathode bipolar plate, such that each bipolar plate contains a flow pattern for reactant and product gas on the one side and a tree-like flow pattern for thermal management on the other side. Adjacent bipolar plates are separated by a separation layer including vertical holes which connect the ends of the highest branching levels of each net. In this manner, the anode side is cooled with colder coolant whereas the cathode side is cooled with preheated, warmer coolant providing a

higher temperature level on the cathode side than on the anode side. Higher temperatures on the cathode side enhance electrochemical reaction rates and increase the saturation pressure of water vapor leading to a reduced amount of condensation which in turn reduces mass transport limitations at high current densities. On the cathode side, the large electrode overpotential and the condensation of water vapor are main performance-limiting factors which are addressed with the proposed concept. Half or part of the tree net may be manufactured on the bipolar plate and the other half on the separation layer. Alternatively, the entire tree net may be manufactured on the bipolar plate only. Such manufacturing issues, although mentioned in passing to indicate possible solutions, are not the main theme of this work which focuses on the basic thermofluidic aspects of the problem. Heat conduction taking place in the solid material between the flow channels (clearly also tractable numerically) is not considered in this work opting for the simple constant heat flux condition on the wall, and only the first net is modeled according to Fig. 2(a)–(c), since the main focus is to demonstrate the power of the tree channel concept leaving further quantification tied to specific applications for future parametric studies.

This net is symmetric with respect to the planes  $y = 0$  and  $z = 0$ . Therefore, for the computational domain drawn in Fig. 2(d), symmetry boundary conditions are applied at  $y = 0$  and  $z = 0$ . A constant velocity profile is applied to the inlet boundary condition. The tree net is cut at the left end of the second and the consequent branching levels and constant mass flow outlet boundary conditions are used to reduce the number of degrees of freedom of the computational model, cf. Fig. 2(d). This configuration of outlet boundary conditions implicitly incorporates the assumption, that at a bifurcation, half of the mass flow is directed to the left and the other half to the right. By modeling an entire tree net with  $m = 4$  for a wide range of inlet Reynolds numbers, it was found that this is a very good assumption indeed, even if for the flow it is not possible to hydrodynamically fully develop before bifurcating. At the highest branching levels, fixed pressure outlet boundary conditions,  $p_{ref} = 0$ , together with zero flux thermal boundary conditions are applied. For heat transfer, a constant fluid inlet temperature profile is set and at the walls of the tree net, a constant heat flux  $q''$  and non-slip boundary conditions are applied.

The serpentine geometry as shown in Fig. 3 has exactly the same heat transfer surface area as the complete fractal geometry with an identical wall heat flux  $q''$ . Its square cross-sectional channels are of constant diameter  $d_0$  which equals to the largest channel diameter in the tree net. The entire serpentine flow pattern covers the same rectangular area as the tree net.

### 3.2. Solution method, grid independency

The set of partial differential equations (6)–(8) with the boundary conditions described above is numerically solved

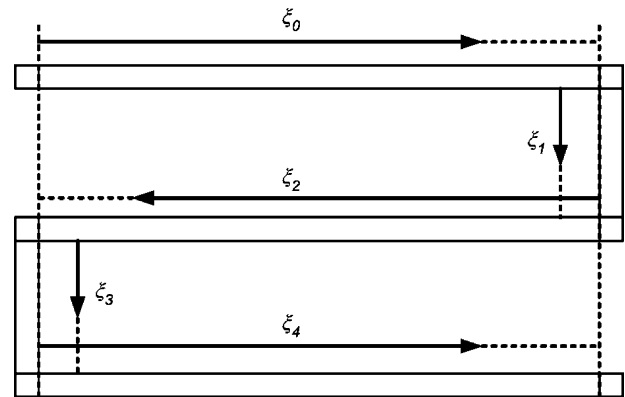


Fig. 3. Serpentine flow pattern with the same heat transfer surface area as the tree net and covering the same rectangular area.

with a finite-volume central scheme on a structured grid using the licensed solver CFD-ACE distributed by CFD Research Corporation of Huntsville, USA. Algebraic multigrid solver is used in conjunction with a convergence criterion of  $1 \times 10^{-10}$ .

The computational grid of the three-dimensional fractal geometry consists of 1,816,800 cells. By increasing the cell number to 2,721,705, practically indistinguishable temperature contours and velocity contours of all three components are obtained when comparing to the results obtained from the coarser grid. By decreasing the cell number to 790,425, small discrepancies are obtained for temperature and velocity contours. The grid resolution of the serpentine flow geometry is consistent with the one of the fractal geometry and it contains 1,063,200 cells.

## 4. Validation

The numerical results are validated with analytical and numerical solutions from literature. For incompressible, laminar and fully developed steady flow of constant viscosity in a square duct, an exact analytical solution [18] can be obtained for the mass and momentum equations (6) and (7). Within this framework, the exact Moody (or Darcy) friction factor  $f$  [18] is given as

$$f Re = 24 \left[ 1 - 192\pi^{-5} \sum_{n=1,3,\dots}^{\infty} n^{-5} \tanh\left(\frac{n\pi}{2}\right) \right]^{-1} \cong 56.908. \quad (9)$$

Iqbal et al. [36] analyzed the H2 boundary condition [18] of rectangular ducts with all four walls heated for a thermally and hydrodynamically fully developed flow with constant fluid properties and neglecting viscous dissipation. For a square duct, they obtained  $Nu = 3.091$  by means of a variational approach. Chandrupatla and Sastri [37] obtained  $Nu = 3.095$  which is in agreement. Their finite difference solutions were computed by using the iterative extrapolated Liebmann method.

For  $Re_{k=0} = 20$ , the flow becomes fully developed both thermally and hydrodynamically in the first channel of the serpentine flow pattern. The present numerical solution of Eqs. (6)–(8), neglecting viscous dissipation in the energy equation like in the references mentioned earlier to facilitate the comparison, yields  $f Re = 56.976$  (+0.118% compared to Ref. [18]) and  $Nu = 3.096$  (+0.162 and +0.0323% compared to Refs. [36,37], respectively), which is in very good agreement with the previously mentioned results.

## 5. Nusslet number and friction factor

In order to investigate the heat transfer and pressure drop characteristics of the tree net and the serpentine flow pattern, the local Nusslet number and local friction factor are determined at each discrete channel cross-section along the flow direction. The local Nusslet number then depends on the position  $\xi_k$  as indicated in Figs. 2(c) and 3, i.e.

$$Nu_k(\xi_k) = \frac{h_k(\xi_k)d_k}{\lambda}, \quad (10)$$

where the subscript  $k$  indicates the branching level in the case of the tree net. With the constant wall heat flux  $q''$ , the local heat transfer coefficient reads

$$h_k(\xi_k) = \frac{q''}{T_{w,m,k}(\xi_k) - T_{m,k}(\xi_k)}, \quad (11)$$

where the mean fluid temperature is given as

$$T_{m,k}(\xi_k) = \frac{\int_0^{\zeta_k, \max} \int_{\eta_k, \min}^{\eta_k, \max} v_{\xi_k, k}(\xi_k, \eta_k, \zeta_k) T_k(\xi_k, \eta_k, \zeta_k) d\eta_k d\zeta_k}{\int_0^{\zeta_k, \max} \int_{\eta_k, \min}^{\eta_k, \max} v_{\xi_k, k}(\xi_k, \eta_k, \zeta_k) d\eta_k d\zeta_k}, \quad (12)$$

and the peripherally averaged wall temperature reads

$$T_{w,m,k}(\xi_k) = \frac{1}{d_k/2} \int_0^{\zeta_k, \max} T_{w,k}(\xi_k, \eta_k, \min, \zeta_k) d\zeta_k + \frac{1}{d_k/2} \int_0^{\zeta_k, \max} T_{w,k}(\xi_k, \eta_k, \max, \zeta_k) d\zeta_k + \frac{1}{d_k} \int_{\eta_k, \min}^{\eta_k, \max} T_{w,k}(\xi_k, \eta_k, \zeta_k, \max) d\eta_k. \quad (13)$$

Herein,  $v_{\xi_k, k}$  is the velocity component in  $\xi_k$ -direction at the  $k$ th branching level. The Reynolds number at the  $k$ th branching level,

$$Re_k \equiv \frac{\rho v_{\xi_k, m, k} d_k}{\mu} \quad (14)$$

with the mean velocity

$$v_{\xi_k, m, k} = \frac{\int_0^{\zeta_k, \max} \int_{\eta_k, \min}^{\eta_k, \max} v_{\xi_k, k}(\xi_k, \eta_k, \zeta_k) d\eta_k d\zeta_k}{\int_0^{\zeta_k, \max} \int_{\eta_k, \min}^{\eta_k, \max} d\eta_k d\zeta_k} = 2^{-k} \beta^{-2k} v_{in}, \quad (15)$$

and the definition of the friction factor,

$$f_k(\xi_k) = -\frac{\partial p_{m,k}}{\partial \xi_k} \frac{2d_k}{\rho v_{\xi_k, m, k}^2}, \quad (16)$$

are used to compute the local  $f_k Re_k(\xi_k)$  which depends on the position along the flow direction. The cross-sectional average of the static pressure

$$p_{m,k}(\xi_k) = \frac{\int_0^{\zeta_k, \max} \int_{\eta_k, \min}^{\eta_k, \max} p_k(\xi_k, \eta_k, \zeta_k) d\eta_k d\zeta_k}{\int_0^{\zeta_k, \max} \int_{\eta_k, \min}^{\eta_k, \max} d\eta_k d\zeta_k} \quad (17)$$

is used to determine the pressure gradient in Eq. (16).

## 6. Numerical results and discussion

The equations governing fluid flow and heat transfer, Eqs. (6)–(8), are numerically solved with respect to the tree and serpentine channel patterns. For each configuration, two cases are considered: The first case is based on  $Re_{k=0} = 20$  and  $Pr = 2.39$  whereas the second case is based on  $Re_{k=0} = 200$  and  $Pr = 2.39$ . This Prandtl number represents the properties of liquid water at 1 bar and 75 °C [38]. The operating temperature range for PEM fuel cells is usually between 65 and 100 °C. For a channel diameter of  $d_0 = 1$  mm at the zeroth branching level, these Reynolds numbers then imply a mean liquid water inlet velocity of 0.774 and 7.74 cm/s, respectively. In this section, laminar mixing, pressure drop, and heat transfer characteristics in the fractal and serpentine flow pattern are discussed and compared to each other. Dimensional results are based on the parameters given in Table 1. Characteristics are plotted for the right-sided branches, cf. Fig. 2(d).

### 6.1. Laminar mixing

As the flow passes through bifurcations, secondary flow motions are initiated as shown in Fig. 4(a) and (b). The higher the flow Reynolds number, the larger their relative magnitude is. Transverse vortices with their axis transverse to the flow in the streamwise direction generate recirculation

Table 1

Properties of liquid water at 1 bar and 75 °C [38]. Boundary conditions and geometry parameters

Density, $\rho$ (kg m <sup>-3</sup> )	975
Dynamic viscosity, $\mu$ (Pa s)	$377 \times 10^{-6}$
Thermal conductivity, $\lambda$ (W m <sup>-1</sup> K <sup>-1</sup> )	0.664
Specific heat capacity, $c_p$ (J kg <sup>-1</sup> K <sup>-1</sup> )	4203
Inlet velocity $v_0$ for $Re_{k=0} = 20$ (cm s <sup>-1</sup> )	0.774
Inlet velocity $v_0$ for $Re_{k=0} = 200$ (cm s <sup>-1</sup> )	7.74
Wall heat flux $q''$ for $Re_{k=0} = 20$ (W m <sup>-2</sup> K <sup>-1</sup> )	776.8
Wall heat flux $q''$ for $Re_{k=0} = 200$ (W m <sup>-2</sup> K <sup>-1</sup> )	7768
Channel diameter $d_0$ at the zeroth branching level (mm)	1.0
Surface area, $S$ (m <sup>2</sup> )	$4.083 \times 10^{-4}$

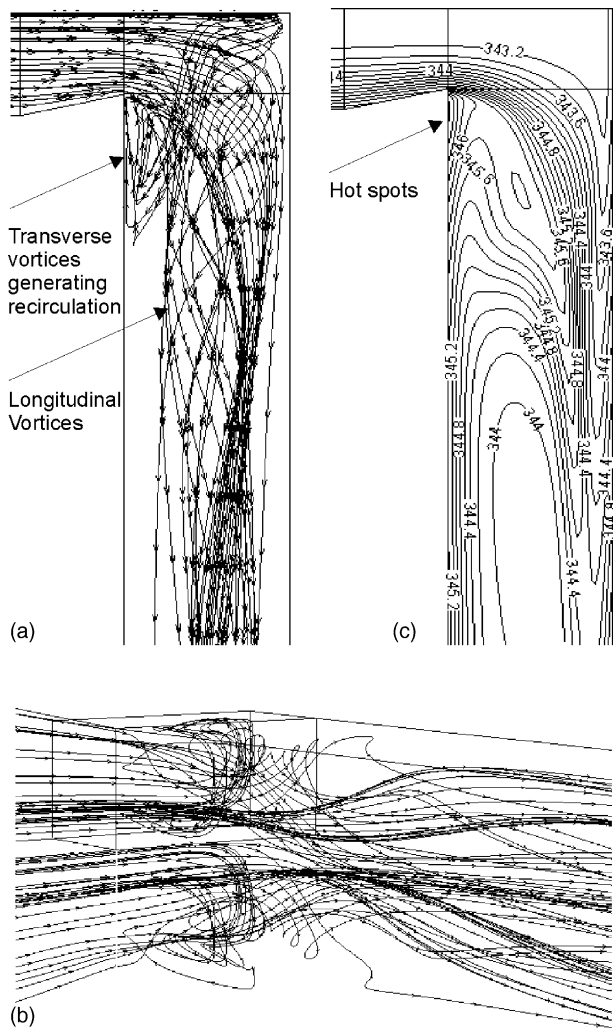


Fig. 4. Laminar mixing at the first bifurcation in the tree net at  $Re_{k=0} = 200$ . (a) Streamlines in top view: transverse vortices with their axis transverse to the flow causing recirculation and longitudinal vortices with their axis along the flow in the streamwise direction. (b) Three-dimensional view. (c) Temperature (K) contours showing hot spots in the recirculation area at  $z = 0$ .

near the inner corners of the bifurcations, where the fluid velocity is much slower than at the outer wall, leading to hot spots in this area, cf. Fig. 4(c). Further, two longitudinal vortices of opposite orientation with their axis along the flow in the streamwise direction are generated, as seen in Fig. 5. Thereby, cold fluid is moved from the outer to the inner wall and finally to the channel core as the strength of the vortices decays with increasing distance from the bifurcation, cf. Fig. 5. With increasing branching level  $k$ , the flow Reynolds number becomes smaller and thereby the initial strength of longitudinal vortices is reduced such that cold fluid is not anymore subject to establish a closed ring with warmer fluid inside this ring.

For the tree net, the distance  $\Delta d_k$  as indicated in Fig. 2(c) has been varied to investigate the dependence of the vortex structures on different geometric configurations of the

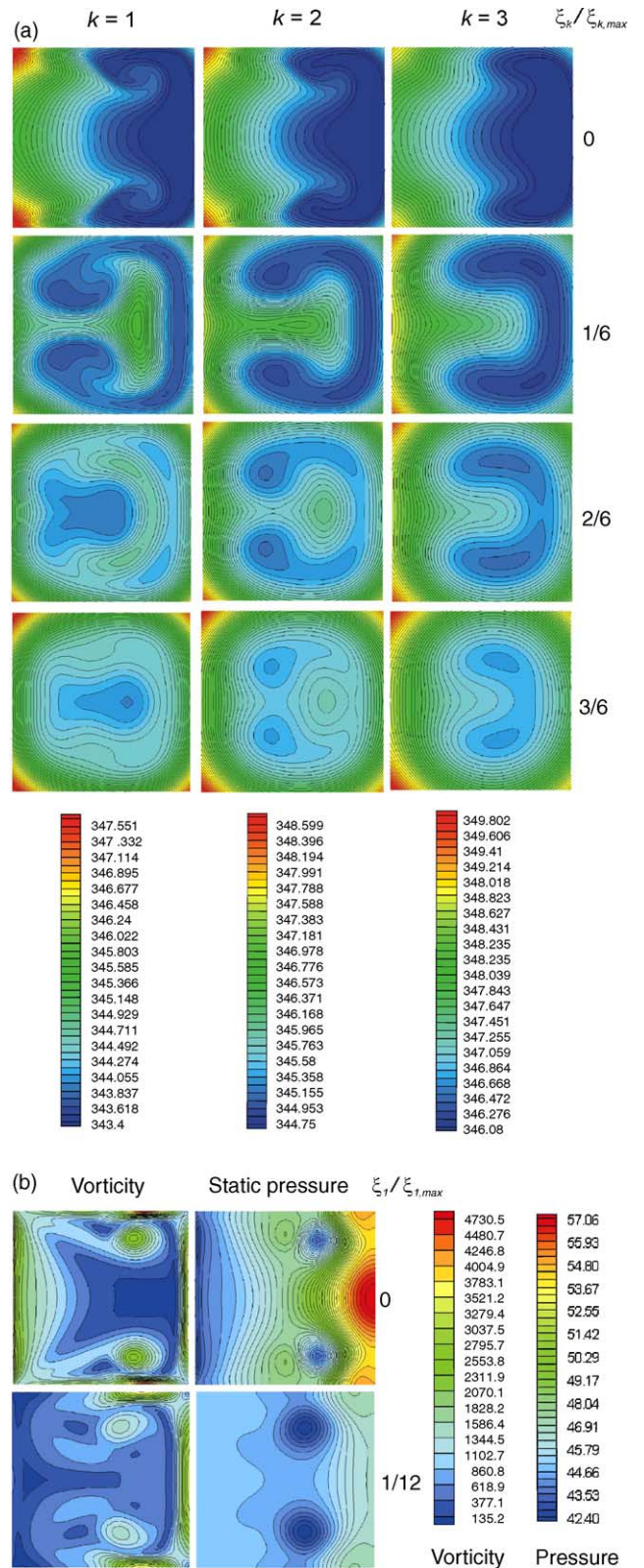


Fig. 5. (a) Temperature (K) contours at four consecutive cross-sections in the first, second, and third branching level of the tree net at  $Re_{k=0} = 200$ . (b) Vorticity ( $s^{-1}$ ) and pressure (Pa) contours at two consecutive cross-sections in the first branching level  $k = 1$  of the tree net at  $Re_{k=0} = 200$ .

converging passages. Identical longitudinal vortex structures of varying strength are found for different values of  $\Delta d_k$ . Herein, the following parameter set has been investigated for the higher Reynolds number level ( $Re_{k=0} = 200$ ):  $\Delta d_k \in (-2a_k, -a_k, 0, a_k, 2a_k)$  with  $a_k = (d_k - d_{k+1})/2$  where the geometry with  $\Delta d_k = a_k$  represents the case being mainly discussed in this study. The strength of the longitudinal vortices increases for larger values of  $\Delta d_k$ , increasing thereby the peak local Nusslet number  $Nu_{k=1,max}$  according to 10.2, 10.9, 12.7, 15.1, and 17.0. However, the pressure drop in the entire tree net increases at the same time according to 50.2, 52.1, 56.1, 65.0, and 87.3 Pa, respectively. Therefore, the effect of thermal mixing can be intensified with increasing values of  $\Delta d_k$  at the cost of additional pressure drop and vice versa. The channel cross-sectional area at the interface of two consecutive branching levels  $k$  and  $k + 1$ , i.e.  $(d_k - 2\Delta d_k)d_{k+1}$ , is reduced with increasing  $\Delta d_k$ .

Therefore, the flow is locally accelerated before entering the higher branching level which causes higher strengths for longitudinal vortices and therefore enhanced thermal mixing. More detailed optimization of the bifurcation geometry at the different branching levels and inlet Reynolds number with respect to both aspects is left to algorithmic optimization studies considering also complexly curved walls. Fluid mixing could also be intensified by different passive methods, e.g. by placing ridges on the floor of the channels at an oblique angle [39] or by inserting C-shaped repeating units in the streamwise direction [40].

### 6.2. Pressure drop

In the tree net, the flow is subject to develop hydrodynamically and thermally in the entrance region of the zeroth branching level due to the constant velocity and temperature

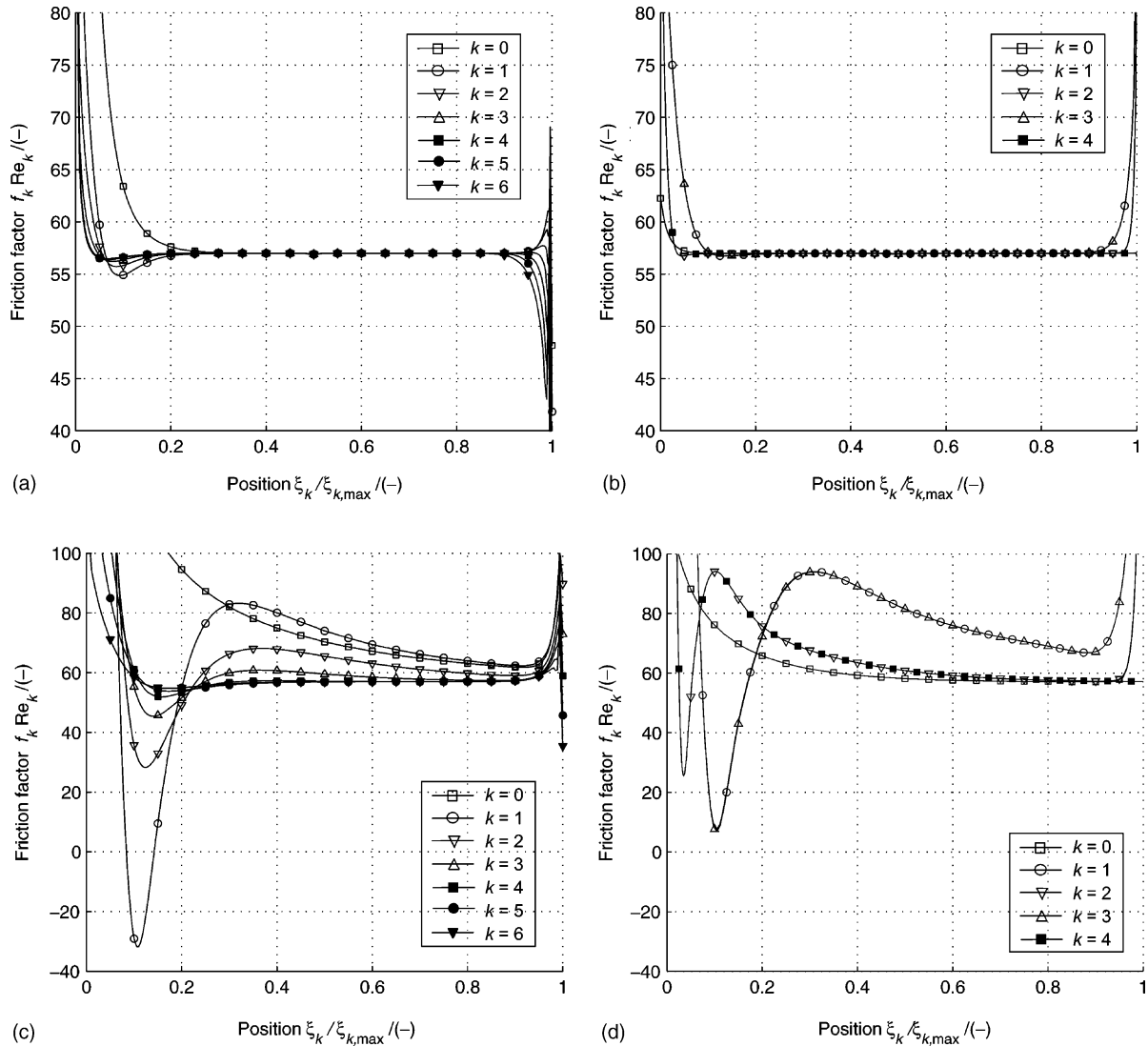


Fig. 6. Friction factor. (a) Tree net with  $Re_{k=0} = 20$ . (b) Serpentine pattern with  $Re_{k=0} = 20$ . (c) Tree net with  $Re_{k=0} = 200$ . (d) Serpentine pattern with  $Re_{k=0} = 200$ .

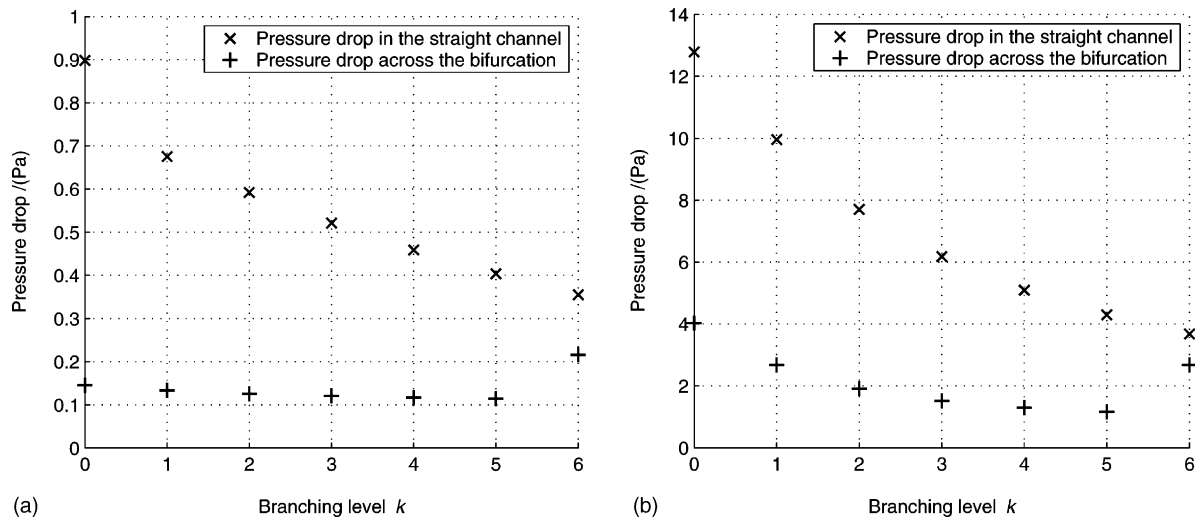


Fig. 7. Pressure drop in the straight channels between  $\xi_{k=0,\min}$  and  $\xi_{k=0,\max}$  (x). Pressure drop across bifurcations between  $\xi_{k,\max}$  and  $\xi_{k+1,\min}$  (+). (a) Tree net with  $Re_{k=0} = 20$ . (b) Tree net with  $Re_{k=0} = 200$ .

profiles at the inlet. At bifurcations, the flow is disturbed and secondary flow motions are initiated which then decay along the next following straight channel portions, such that the flow tends to develop again before reaching the next bifurcation. In the serpentine channels, the flow is subject to develop in the straight channels whereas it is disturbed again at each turn.

For  $Re_{k=0} = 20$ , the hydrodynamic development lengths are small compared to the length of the corresponding straight channels. This is seen in Fig. 6(a) and (b) from the course of the friction factor which evens out at a certain level when the flow becomes fully developed. In the tree net, the pressure drop across the first bifurcation (0.145 Pa) is 16.2% of the pressure drop between  $\xi_{k=0,\min}$  and  $\xi_{k=0,\max}$  in the straight channel of the zeroth branching level (0.898 Pa), cf. Fig. 7(a). Herein, the cross-sectional average of the static pressure at  $\xi_{k,\max}$  is subtracted from the corresponding value at  $\xi_{k+1,\min}$  to evaluate the pressure drop across a bifurcation. The pressure drop across the sixth bifurcation (0.114 Pa) is 28.3% of the pressure drop in the straight channel of the fifth branching level (0.404 Pa). Consequently, at the higher branching levels, the contribution of the pressure drop obtained across bifurcations becomes more important compared to the pressure drop in the straight channels, as seen from Fig. 7(a). This fact is due to the growing ratio between the channel diameter and the channel length when going to higher branching levels, i.e.  $d_{k+1}/L_{k+1} = (\beta/\gamma)d_k/L_k \cong 1.12d_k/L_k$ . Therefore, analytical approaches [6] where the laminar flow is assumed to be hydrodynamically fully developed everywhere and where the effect of bifurcation on pressure drop is neglected, are only adequate if the hydrodynamic development lengths are very small compared to the length of the straight channels, i.e. for low Reynolds numbers, high  $L_k/d_k$  ratios and for the lower branching levels. For the entire tree net, the resulting overall pressure drop (4.88 Pa) is only 56.9% of the

pressure drop obtained from the corresponding serpentine flow pattern (8.57 Pa) having exactly the same surface area  $S$ . As a further comparison, the pressure drop in a single square cross-sectional straight channel with diameter  $d_0$  and surface area  $S$  can be obtained analytically from Eqs. (9) and (16) by assuming fully developed flow. A value of 8.48 Pa is found for such a straight channel flow which is only slightly below the pressure drop in the serpentine flow pattern but at the same time almost double the pressure drop in the tree net.

For  $Re_{k=0} = 200$ , the flow does not fully develop any more at the lower branching levels  $k = 0, 1, 2$  of the tree net, as seen from Fig. 6(c). In the serpentine pattern, the flow develops in the long straight channels,  $k = 0, 2, 4$ , such that the friction factor variations in the shorter channels  $k = 1$  and  $k = 3$  are similar to each other, cf. Fig. 6(d). The pressure drop across the first bifurcation in the tree net (4.03 Pa) is 31.5% of the pressure drop in the straight channel of the zeroth branching level (12.8 Pa), cf. Fig. 7(b). The pressure drop across the fifth bifurcation (1.29 Pa) is 25.4% of the pressure drop in the straight channel of the fourth branching level (5.09 Pa). Here, the relative importance of the bifurcation pressure drop does not monotonically increase with increasing branching levels, since the flow does not develop fully at the lower branching levels leading to a higher relative pressure drop from bifurcations at these branching levels. For  $k = 0$  to  $k = 5$ , these ratios are 31.5, 26.9, 24.8, 24.5, 25.4, and 27.1%, respectively. As expected, the ratios increase again after the third branching level where the flow tends to develop more approaching fully developed state before bifurcating. The overall pressure drop resulting from the entire tree net (65.0 Pa) is only 55.1% of the pressure drop obtained from the corresponding serpentine flow pattern (118 Pa). When comparing the overall pressure drop of the tree net at  $Re_{k=0} = 20$  (4.88 Pa) to the one at  $Re_{k=0} = 200$  (65.0 Pa), an increase by a factor of 13.3 is identified.

For fully developed flow and neglecting effects from bifurcations, a factor of 10 would be expected. When considering again a single straight channel with fully developed flow, a pressure drop of 84.8 Pa is found analytically, which is substantially below the pressure drop in the serpentine flow pattern and at the same time also substantially above the pressure drop in the tree net.

In conclusion, the relative effect of pressure drop from bifurcations becomes more dominant at the higher branching levels. In spite of the large number of bifurcations in the tree net compared to a much lower number of turns in the serpentine flow pattern, the tree net proves significantly beneficial in terms of pressure drop.

### 6.3. Heat transfer

In the tree net, the flow becomes thermally fully developed at each branching level for  $Re_{k=0} = 20$ . This is seen

in Fig. 8(a) from the variation of the Nusslet number which evens out at a certain level when the flow is subject to develop. The same applies to the serpentine flow pattern, cf. Fig. 8(b). As expected, the heat transfer coefficient  $h_k$  in the thermally fully developed region scales with  $h_k \propto 1/d_k$  which implies that in the highest level of the tree net a more than four times higher heat transfer coefficient can be obtained than in the serpentine flow pattern, as seen from Fig. 9(a) and (b). Therefore, a smaller temperature difference is needed to transfer the same heat flux from the channel walls to the bulk fluid at the higher branching levels of the tree net. Due to the constant wall heat flux boundary condition used in this study and since the channel diameter gets smaller when going to higher branching levels, the length-specific heat transfer rate to the fluid decreases from one branching level to the next higher one, i.e. by the factor  $\beta \cong 0.794$ . The heat transfer rate to a single channel of the branching level  $k + 1$  is  $\gamma\beta \cong 0.561$  times smaller than the

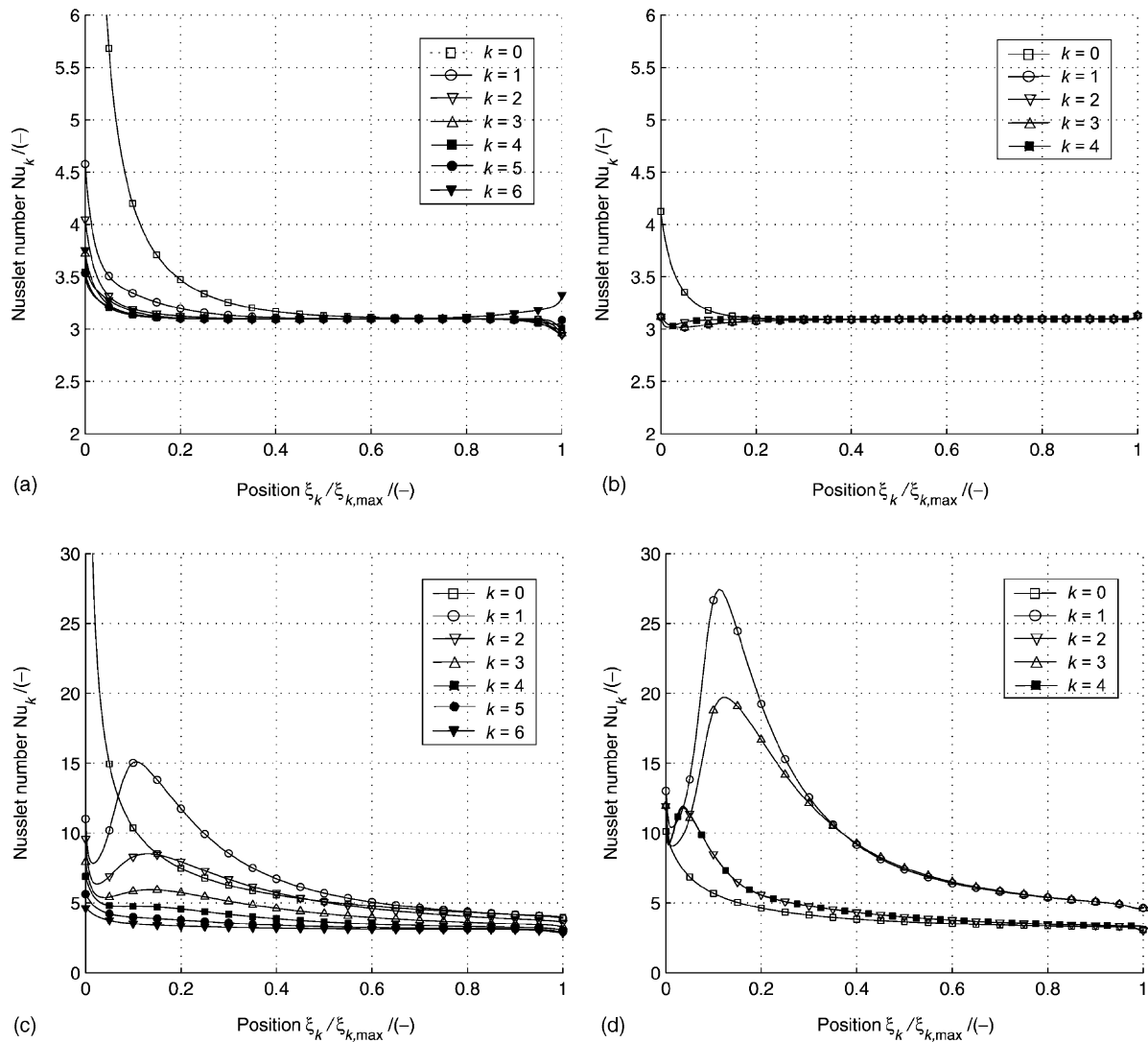


Fig. 8. Nusslet Number. (a) Tree net with  $Re_{k=0} = 20$ . (b) Serpentine pattern with  $Re_{k=0} = 20$ . (c) Tree net with  $Re_{k=0} = 200$ . (d) Serpentine pattern with  $Re_{k=0} = 200$ .

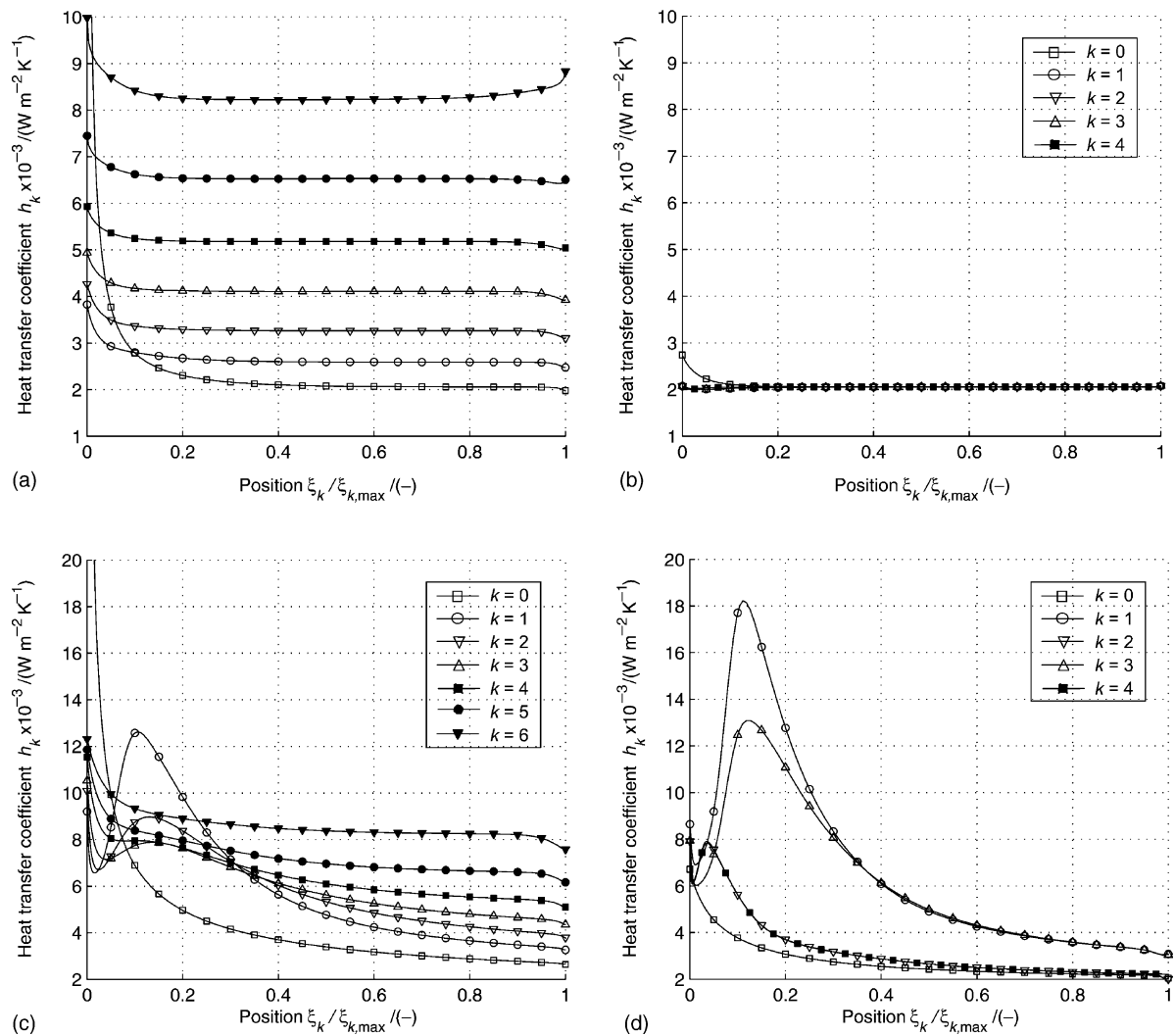


Fig. 9. Heat transfer coefficient. (a) Tree net with  $Re_{k=0} = 20$ . (b) Serpentine pattern with  $Re_{k=0} = 20$ . (c) Tree net with  $Re_{k=0} = 200$ . (d) Serpentine pattern with  $Re_{k=0} = 200$ .

heat transfer rate to a single channel of the branching level  $k$ . However, the heat transfer rate to all the channels of the branching level  $k + 1$  is  $2\gamma\beta \cong 1.12$  times larger than the heat transfer rate to all the channels of the branching level  $k$ . Only for large  $L_k/d_k$  ratios and low Reynolds numbers or if the thermal development length can be neglected with respect to the channel length  $L_k$ , the assumption of constant Nusslet number to compute the heat transfer capability of the tree net is adequate.

For a 10 times higher inlet Reynolds number to the tree net, i.e.  $Re_{k=0} = 200$ , the flow does not thermally develop any more, except at the highest branching levels, as seen from Fig. 8(c). When the flow passes through the bifurcation, secondary flow motions are initiated that degenerate the thermal boundary layer. This effect causes high-temperature fluid, which is captivated near the walls in the fully developed region, to mix with low-temperature fluid from the channel core, as illustrated in Fig. 5. This convective thermal mixing effect provides a smaller difference

between the mean wall temperature  $T_{w,m,k}$  and the mean fluid temperature  $T_{m,k}$  and, due to the constant wall heat flux, leads to an increase of the local Nusslet number  $Nu_k$  in the straight channels right after bifurcations, cf. Fig. 8(c). The effect of thermal mixing caused by secondary flow motions and reinitiated at each bifurcation becomes dominant at this inlet Reynolds number level and the Nusslet number reaches a peak value of  $Nu_{k=1} = 15.1$  at a distance  $\xi_{k=1}/\xi_{k=1,\text{max}} = 0.106$  after bifurcating. This value is almost five times larger than the Nusslet number of a thermally and hydrodynamically fully developed flow. For higher branching levels, the peak Nusslet number decreases from one level to the next higher. The effectiveness of thermal mixing initiated at bifurcations depends on the Reynolds number. It is improved for increasing Reynolds numbers and vice versa. Since the Reynolds number decreases from one branching level to the next higher one, i.e. according to  $Re_{k+1}/Re_k = 1/(2\beta) \cong 0.630$ , thermal mixing becomes less effective at the higher branching levels which

manifests itself in the above-mentioned decrease of the peak Nusslet number from one level to the next higher one. The local heat transfer coefficient increases from one branching level to the next higher with high local peaks due to thermal mixing, cf. Fig. 9(c). In many applications, e.g. fuel cell cooling and electronics cooling, a thermofluidic design for thermal management is subject to the constraint of a maximum temperature difference within the considered system. Therefore, when attempting to transfer larger heat fluxes under such a constraint, higher heat transfer coefficients are required since they allow a certain heat flux to be transferred at a smaller temperature difference. In this respect, the tree net proves significantly beneficial, as shown in Fig. 9(a)–(d).

The higher the branching level, the more beneficial it proves. Hence, when considering a single tree net, a higher maximum heat rate could be transferred than with the serpentine flow pattern, if a certain maximum temperature difference is imposed on the two systems, as seen from

Fig. 10(a)–(d). On the other hand, reduced temperature differences needed to transfer a constant wall heat flux at the higher branching levels imply a reduced maximum temperature difference within the entire system. At  $Re_{k=0} = 200$ , a maximum temperature difference between  $T_{w,max}$  and  $T_{m,min}$  of 12.0 K is obtained from the tree net, compared to the corresponding value of 16.0 K from the serpentine flow pattern. For  $Re_{k=0} = 20$  and with a 10 times lower wall heat flux than in the higher Reynolds number case, these two values are closer together, as seen from Fig. 10(a)–(d). The higher the wall heat flux and the larger the total number of branching levels, the more advantageous the single tree net with respect to small temperature differences. Providing a uniform temperature distribution is one of the previously mentioned important requirements for effective thermal management in polymer electrolyte fuel cells.

For a double tree net, this argumentation no longer holds. The same maximum temperature difference will be obtained

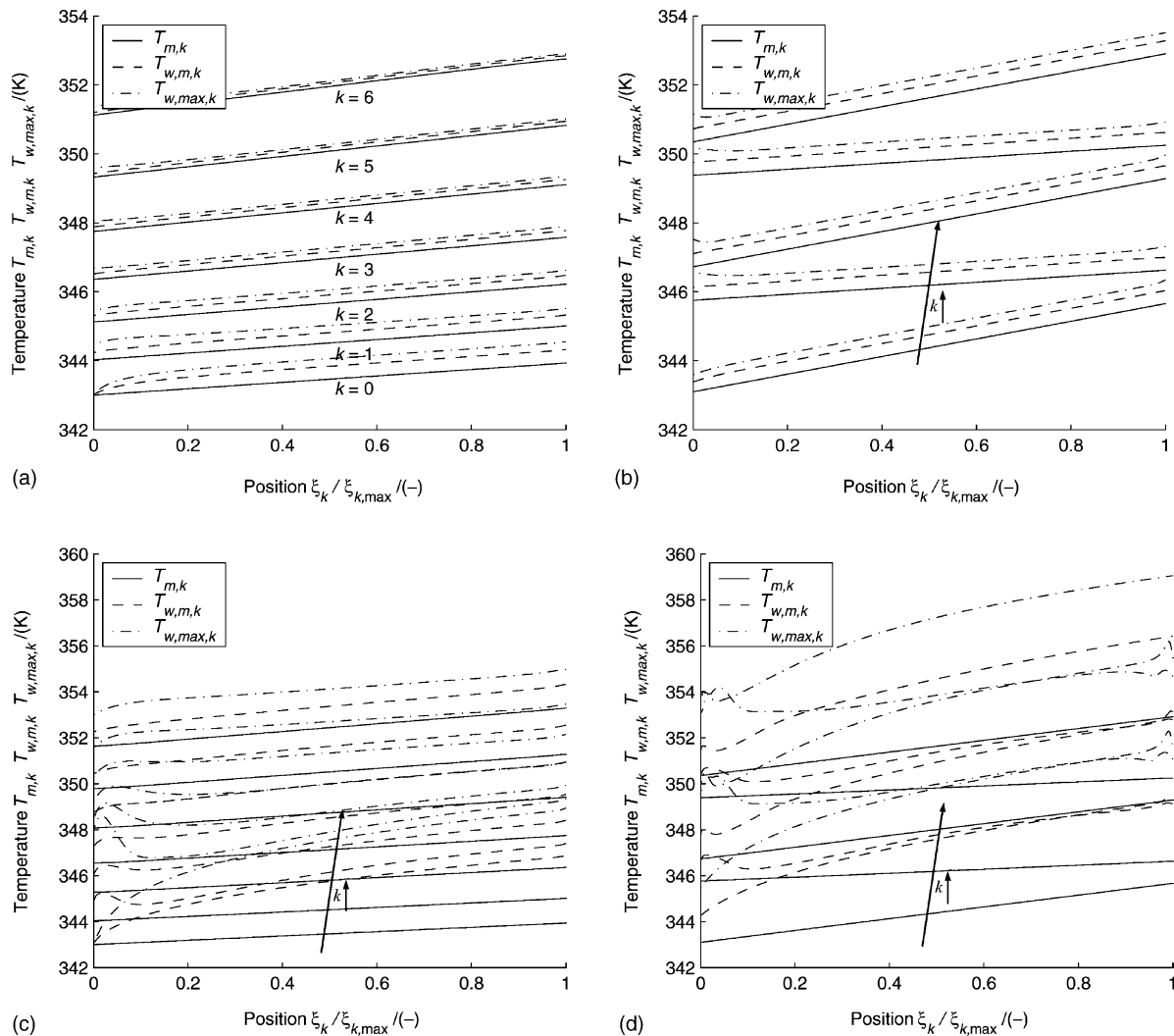


Fig. 10. Mean fluid temperature, mean wall temperature, and maximum wall temperature. (a) Tree net with  $Re_{k=0} = 20$ ,  $q'' = 776.8 \text{ W m}^{-2} \text{ K}^{-1}$ . (b) Serpentine pattern with  $Re_{k=0} = 20$ ,  $q'' = 776.8 \text{ W m}^{-2} \text{ K}^{-1}$ . (c) Tree net with  $Re_{k=0} = 200$ ,  $q'' = 7768 \text{ W m}^{-2} \text{ K}^{-1}$ . (d) Serpentine pattern with  $Re_{k=0} = 200$ ,  $q'' = 7768 \text{ W m}^{-2} \text{ K}^{-1}$ .

from a double tree net and from a serpentine flow pattern of identical surface area and with identical constant wall heat flux. However, it is still thermodynamically desirable to transfer a certain heat flux with a small temperature difference because of smaller corresponding entropy generation. In addition, there is room for the transfer of higher heat fluxes if needed, by increasing the temperature difference. As an example, a substantially higher overall heat transfer rate could be obtained from the single or double tree net compared to the serpentine flow pattern of the same surface area, if instead of the constant wall heat flux a constant temperature difference,  $T_{w,m,k} - T_{m,k} = \text{const.}$ , could be maintained along the entire channel system. This can be seen from the variation of the mean wall temperature and the mean fluid temperature in Fig. 10(a) and (b): In the fully developed regions of the tree net, the difference between the mean wall temperature and the mean fluid temperature decreases from one branching level to the next higher whereas in the serpentine pattern this difference remains constant. Enforcing such a constant temperature difference in all the branching levels of the tree net would imply larger heat fluxes at the higher branching levels and therefore the curves indicating the variation of the mean fluid temperature would get steeper from one branching level to the next higher. Hence, under such conditions, a higher mean fluid temperature would be obtained at the end of the tree net than at the end of the serpentine pattern. Alternatively, in trying to get the same mean fluid temperature at the end of both configurations, a tree net with a smaller number of branching levels would be necessary which would further reduce the amount of pressure drop in the tree net.

Finally, it is worth mentioning that the effect of viscous dissipation can be safely neglected in the cases considered so far, as seen from the local Brinkman numbers, which are in the order of  $1 \times 10^{-6}$ . This was also numerically verified by simply dropping the viscous dissipation term out of the energy equation and then comparing with the former results.

## 7. Conclusions

A thorough three-dimensional forced convection model was presented for two geometrical channel configurations with constant wall heat flux: a tree-like net and a serpentine flow pattern having the same surface area. The tree network configuration represents the main novel concept of this paper for cooling systems in applications such as fuel cells and electronic devices. The serpentine configuration is typical in the cooling of PEM fuel cells and provides a basis of comparison.

It is found that the tree net with six branching levels generates almost half the pressure drop than the corresponding serpentine flow pattern having the same surface area and inlet Reynolds number. The effect of pressure drop from bifurcations and turns is substantial and should not be neglected for simplicity by using fully developed flow friction factors

in the considered cases. Although the number of bifurcations in the tree net is larger than the number of turns in the serpentine flow pattern, from which one would expect a lower pressure drop from the serpentine flow pattern, the tree net proves to be markedly beneficial in terms of pressure drop.

In addition to hydrodynamic advantages, the tree net further provides a larger heat transfer capability than the serpentine pattern. Laminar mixing by secondary flow motions initiated at bifurcations causes substantially improved local Nusslet numbers. Much higher heat transfer coefficients are obtained for the tree net which implies that at the higher branch levels, a certain heat flux can be transferred with a smaller temperature difference. A much higher heat transfer rate could be obtained for the tree net by increasing this temperature difference. If for the water temperature it is possible to reach the boiling temperature, i.e. if the cell would be operated above this temperature level, evaporation can occur, leading to different regimes of two-phase flow in the cooling channels. This case was not investigated in the present study which focused on the single-phase flow regime.

Due to their intrinsic advantage with respect to both heat transfer and pressure drop, tree-like nets have the potential to significantly aid the thermal management in polymer electrolyte fuel cells at different length scales as well as in other thermal systems.

## Acknowledgements

This work has been supported by the Swiss Federal Office of Energy (BFE) under contract No. 87100 (program manager Dr. A. Hintermann). CFD Research Corporation of Huntsville, USA, is acknowledged for allowing the use of their software.

## References

- [1] A. Bejan, From heat transfer principles to shape and structure in nature: constructal theory, *J. Heat Transfer* 122 (3) (2000) 430–449.
- [2] A. Bejan, *Shape and Structure, From Engineering to Nature*, Cambridge University Press, Cambridge, 2000.
- [3] G.B. West, J.H. Brown, B.J. Enquist, A general model for the origin of allometric scaling laws in biology, *Science* 276 (5309) (1997) 122–126.
- [4] A. Bejan, M.R. Errera, Deterministic tree networks for fluid flow: geometry for minimal flow resistance between a volume and a point, *Fractals* 5 (4) (1997) 685–695.
- [5] A. Bejan, The tree of convective heat streams: its thermal insulation function and the predicted 3/4-power relation between body heat losses and body size, *Int. J. Heat Mass Transfer* 44 (4) (2001) 699–704.
- [6] Y. Chen, P. Cheng, Heat transfer and pressure drop in fractal tree-like microchannel nets, *Int. J. Heat Mass Transfer* 45 (13) (2002) 2643–2648.
- [7] B. Palm, Heat transfer in microchannels, *Microscale Thermophys. Eng.* 5 (3) (2001) 155–175.
- [8] C.M. Ho, Y.C. Tai, Micro-electro-mechanical-systems (MEMS) and fluid flows, *Ann. Rev. Fluid Mech.* 30 (1998) 579–612.

- [9] N.T. Obot, Toward a better understanding of friction and heat/mass transfer in microchannels—a literature review, *Microscale Thermophys. Eng.* 6 (3) (2002) 155–173.
- [10] X.F. Peng, G.P. Peterson, Convective heat transfer and flow friction for water flow in microchannel structures, *Int. J. Heat Mass Transfer* 39 (12) (1996) 2599–2608.
- [11] S.M. Flockhart, R.S. Dhariwal, Experimental and numerical investigation into the flow characteristics of channels etched in (100) silicon, *J. Fluids Eng.* 120 (2) (1998) 291–295.
- [12] R.L. Webb, M. Zhang, Heat transfer and friction in small diameter channels, *Microscale Thermophys. Eng.* 2 (3) (1998) 189–202.
- [13] T.M. Adams, S.I. Abdel-Khalik, S.M. Jeter, Z.H. Qureshi, An experimental investigation of single-phase forced convection in microchannels, *Int. J. Heat Mass Transfer* 41 (6–7) (1998) 851–857.
- [14] W. Qu, G. Mohiuddin Mala, D. Li, Heat transfer for water flow in trapezoidal silicon microchannels, *Int. J. Heat Mass Transfer* 43 (21) (2000) 3925–3936.
- [15] J. Judy, D. Maynes, B.W. Webb, Characterization of frictional pressure drop for liquid flows through microchannels, *Int. J. Heat Mass Transfer* 45 (17) (2002) 3477–3489.
- [16] D. Brutin, L. Tadrist, Experimental friction factor of a liquid flow in microtubes, *Phys. Fluids* 15 (3) (2003) 653–661.
- [17] Z.Y. Guo, Z.X. Li, Size effect on microscale single-phase flow and heat transfer, *Int. J. Heat Mass Transfer* 46 (1) (2003) 149–159.
- [18] R.K. Shah, A.L. London, *Laminar Flow Forced Convection in Ducts*, Advances in Heat Transfer, Academic Press, New York, 1978.
- [19] G. Mohiuddin Mala, D. Li, Flow characteristics of water in microtubes, *Int. J. Heat Fluid Flow* 20 (2) (1999) 142–148.
- [20] G. Tunc, Y. Bayazitoglu, Heat transfer in rectangular microchannels, *Int. J. Heat Mass Transfer* 45 (4) (2002) 765–773.
- [21] W. Qu, I. Mudawar, Experimental and numerical study of pressure drop and heat transfer in a single-phase micro-channel heat sink, *Int. J. Heat Mass Transfer* 45 (12) (2002) 2549–2565.
- [22] W. Qu, I. Mudawar, Analysis of three-dimensional heat transfer in micro-channel heat sinks, *Int. J. Heat Mass Transfer* 45 (19) (2002) 3973–3985.
- [23] C.Y. Zhao, T.J. Lu, Analysis of microchannel heat sinks for electronics cooling, *Int. J. Heat Mass Transfer* 45 (24) (2002) 4857–4869.
- [24] K.C. Toh, X.Y. Chen, J.C. Chai, Numerical computation of fluid flow and heat transfer in microchannels, *Int. J. Heat Mass Transfer* 45 (26) (2002) 5133–5141.
- [25] G. Mohiuddin Mala, D. Li, J.D. Dale, Heat transfer and fluid flow in microchannels, *Int. J. Heat Mass Transfer* 40 (13) (1997) 3079–3088.
- [26] C. Yang, D. Li, J.H. Masliyah, Modeling forced liquid convection in rectangular microchannels with electrokinetic effects, *Int. J. Heat Mass Transfer* 41 (24) (1998) 4229–4249.
- [27] L. Ren, W. Qu, D. Li, Interfacial electrokinetic effects on liquid flow in microchannels, *Int. J. Heat Mass Transfer* 44 (16) (2001) 3125–3134.
- [28] S. Yu, T.A. Ameel, Slip-flow heat transfer in rectangular microchannels, *Int. J. Heat Mass Transfer* 44 (22) (2001) 4225–4234.
- [29] J. Yang, D.Y. Kwok, Microfluid flow in circular microchannel with electrokinetic effect and Navier’s slip condition, *Langmuir* 19 (2003) 1047–1053.
- [30] D. Maynes, B.W. Webb, Fully developed electro-osmotic heat transfer in microchannels, *Int. J. Heat Mass Transfer* 46 (8) (2003) 1359–1369.
- [31] C.P. Tso, S.P. Mahulikar, The use of the Brinkman number for single phase forced convective heat transfer in microchannels, *Int. J. Heat Mass Transfer* 41 (12) (1998) 1759–1769.
- [32] C.P. Tso, S.P. Mahulikar, The role of the Brinkman number in analysing flow transitions in microchannels, *Int. J. Heat Mass Transfer* 42 (10) (1999) 1813–1833.
- [33] C.P. Tso, S.P. Mahulikar, Experimental verification of the role of Brinkman number in microchannels using local parameters, *Int. J. Heat Mass Transfer* 43 (10) (2000) 1837–1849.
- [34] D.A.W. Thompson, *On Growth and Form*, Cambridge University Press, Cambridge, UK, 1942.
- [35] C.D. Murray, The physiological principle of minimal work in vascular system, and the cost of blood-volume, *Proc. Acad. Natl. Sci.* 12 (1926) 207–214.
- [36] M. Iqbal, A.K. Khatry, B.D. Aggarwala, On the second fundamental problem of combined free and forced convection through vertical non-circular ducts, *Appl. Sci. Res.* 26 (3–4) (1972) 183–208.
- [37] A.R. Chandrupatla, V.M.K. Sastri, Laminar forced convection heat transfer of a non-Newtonian fluid in a square duct, *Int. J. Heat Mass Transfer* 20 (12) (1977) 1315–1324.
- [38] E. Schmidt, *Properties of Water and Steam in SI-Units*, Springer, New York, 1989.
- [39] A.D. Stroock, et al., Chaotic mixer for microchannels, *Science* 295 (5555) (2002) 647–651.
- [40] R.H. Liu, et al., Passive mixing in a three-dimensional serpentine microchannel, *J. Microelectromech. Syst.* 9 (2) (2000) 190–197.